JOURNAL OF GUIDANCE, CONTROL, AND DYNAMICS
Vol. 37, No. 2, March–April 2014

N-Impulse Formation Flying Feedback Control Using Nonsingular Element Description

Paul V. Anderson* and Hanspeter Schaub†
University of Colorado, Boulder, Colorado 80309

DOI: 10.2514/1.60766

An *N*-impulse feedback control strategy is developed to mitigate errors in a set of nonsingular orbit element differences between a chief and deputy spacecraft. Although suitable for general, elliptic chief orbits, this strategy is motivated by relative orbit control in the geostationary regime, in which nonsingular element descriptions are especially convenient. The Gauss variational equations for this nonsingular set are developed as a basis for the *N*-impulse feedback control strategy, which assumes piecewise constant element errors evaluated once per orbit. The *N* corrective impulses are applied at uniform intervals in true anomaly, and the magnitudes thereof are determined with a swift numerical method. Two examples demonstrate that this method is proficient in helping to detect fuel-optimal burn locations for general formation and element difference corrections.

I. Introduction

SPACECRAFT formation flight presents a challenging controls problem that has been extensively studied in the literature. In the dynamic environment of Earth, naturally occurring drift renders periodic formation-keeping maneuvers essential to operations — a myriad of analytical and numerical control formulations have therefore been developed to perform general formation maintenance and reconfiguration. In particular, Schaub and Alfriend [1] develop an impulsive control strategy using the orbit element difference description of relative motion [2,3] to stabilize the motion of a deputy craft relative to the chief spacecraft. Relative orbit errors are evaluated once per revolution using classical Keplerian elements, and a near-fuel-optimal impulsive firing strategy is computed to correct these formation errors over one revolution. With a piecewise constant orbit element assumption, and the absence of perturbations in the control development, this analytical firing technique will not nullify all of the formation errors within one revolution — rather, orbit element difference errors must be re-evaluated prior to each orbit, and the impulsive scheme reapplied. One of the challenges of this method is that it is developed using a classical Keplerian element description that is near-singular for geostationary (GEO) orbits. With renewed interest in on-orbit servicing and refueling applications, the problems of relative motion and intersatellite rendezvous, especially in the GEO regime, acquire a renewed importance [4–6]. In many studies, propagation and estimation strategies are implemented with these classical elements, or Cartesian positions and velocities, to characterize relative spacecraft motion. However, these representations are nonideal for motion at GEO: Keplerian elements are not well-defined for near-circular and near-equatorial orbits typical of the GEO regime, and rapidly-changing Cartesian states mask the near-linearity of geosynchronous motion [7]. Therefore, nonsingular element sets are most desirable for describing relative motion in the GEO regime. In this study, the variational equations for a nonsingular element set are derived, and implemented as the foundation of an impulsive feedback strategy that seeks to minimize control effort for formation maintenance applications, or more generally, solutions to the orbital correction problem. Note that although the numerical examples that will demonstrate this *N*-impulse strategy consider a GEO formation flying problem, the presented nonsingular element formulation is suitable for all orbit regimes, especially those involving orbits that are near-circular and/or near-equatorial.

Impulsive feedback control methodologies for formation flying applications have been extensively studied in the literature. Vadali et al. [8] present a fuel-optimal technique for controlling mean orbit element errors using up to six impulses of arbitrary magnitude and direction. Choi et al. [9] develop a multi-impulse control strategy using energy matching and the relative angular momentum vector, and Tong et al. [10] present an impulsive relative orbit control method tailored for measurements of the relative range and line-of-sight angles. Prussing and Chiu [11] and Shen and Tsiotras [12] treat the problem of optimal, time-fixed rendezvous between two spacecraft on circular orbits, using optimal control theory and multiple revolution Lambert solutions, respectively, to determine the required impulse magnitudes. Several studies in the literature (see, for example, [13,14]) rely upon complex, global optimization strategies such as genetic algorithms to determine optimal impulsive orbit corrections.

In the general orbit correction problem, the initial conditions for complex optimization routines are nonintuitive and difficult to determine. To alleviate this potential difficulty, this study presents a time-fixed, *N*-impulse strategy to determine appropriate initial conditions for more complicated trajectory optimization algorithms, costing minimal computing time. This *N*-impulse method is a generalization of the impulsive feedback control presented in [1] that harnesses nonsingular elements instead of the classical elements. However, in contrast to the method in [1], the algebra associated with these nonsingular elements renders finding optimal firing times analytically a very challenging task for general relative orbit errors. Thus, it is of interest to formulate a new method to solve a simple, numerical fuel-minimization problem subject to linear constraints, to rapidly detect locations at which corrective impulses should be performed. Thanks to the nonsingular element description implemented in this formulation, the new impulsive formation control technique is applicable for general orbits. Furthermore, the setup to determine optimal impulse locations is greatly simplified by transforming the control evaluation into a constrained linear algebra problem. Simulations are used to study the performance of the developed *N*-impulse feedback control technique in the presence of perturbations that are unmodeled in the control formulation.

II. Development of Gaussian Variational Equations

This study implements an element difference description [2] of relative motion, using the nonsingular set $\boldsymbol{e} \equiv (a, \xi, \eta, \zeta, \psi, \lambda)$, where

Presented as Paper 2012-4585 at the AIAA/AAS Astrodynamics Specialist Conference, Minneapolis, MN, 13–16 August 2012; received 15 October 2012; revision received 5 June 2013; accepted for publication 21 June 2013; published online 12 February 2014.

*Graduate Student, Department of Aerospace Engineering Sciences, 429 UCB. Student Member AIAA.

†Professor, H. Joseph Smead Fellow, Associate Chair of Graduate Affairs, Department of Aerospace Engineering Sciences, 429 UCB. Associate Member AIAA.

a is the semi-major axis of the orbit and the other parameters are defined by [15]

$$\begin{aligned}\xi &\equiv e\ \sin(\omega+\Omega)\\ \eta &\equiv e\ \cos(\omega+\Omega)\\ \zeta &\equiv \sin(i/2)\sin(\Omega)\\ \psi &\equiv \sin(i/2)\cos(\Omega)\\ \lambda &\equiv f+\omega+\Omega\end{aligned} \tag{1}$$

The classical Keplerian elements of eccentricity e, inclination i, right ascension of ascending node Ω, argument of periapsis ω, and true anomaly f are thereby used to assemble the nonsingular set presented in Eq. (1). The inertial Cartesian state of the chief and deputy spacecraft may be readily mapped to the classical elements, which are thereafter transformed to this nonsingular set using the preceding formulation. Note that this nonsingular set is a modified variant of the equinoctial element set established by Broucke and Cefola [16], in which the $\tan(i/2)$ factor inherent to the ζ and ψ elements has been replaced with a $\sin(i/2)$ factor to eliminate the singularity occurring at the retrograde inclination $i = 180$ deg. The nonsingular set $\boldsymbol{e}$ furthermore differs from the conventional equinoctial set by implementing the true anomaly f (instead of the mean anomaly) in the definition of the true longitude parameter λ, to simplify the required derivations. The modified elements given in Eq. (1) are well-defined for zero eccentricity and inclination, and are therefore suitable for describing deputy motion relative to chief orbits in regimes such as GEO. Appendix A presents the forward linear mapping from differences in the nonsingular element set in Eq. (1) to the corresponding Cartesian state of the deputy spacecraft in the Hill frame of the chief spacecraft.

The Gaussian variational equations for nonconservative perturbations to the nonsingular orbital elements are developed to characterize the sensitivities of this set to thrusting events, as this formulation quantifies rates of change of these elements in the presence of nonconservative accelerations. Differentiating Eq. (1):

$$\frac{\mathrm{d}\xi}{\mathrm{d}t} = \sin(\omega+\Omega)\frac{\mathrm{d}e}{\mathrm{d}t} + \eta\left(\frac{\mathrm{d}\omega}{\mathrm{d}t}+\frac{\mathrm{d}\Omega}{\mathrm{d}t}\right) \tag{2}$$

$$\frac{\mathrm{d}\eta}{\mathrm{d}t} = \cos(\omega+\Omega)\frac{\mathrm{d}e}{\mathrm{d}t} - \xi\left(\frac{\mathrm{d}\omega}{\mathrm{d}t}+\frac{\mathrm{d}\Omega}{\mathrm{d}t}\right) \tag{3}$$

$$\frac{\mathrm{d}\zeta}{\mathrm{d}t} = \frac{1}{2}\cos(i/2)\sin(\Omega)\frac{\mathrm{d}i}{\mathrm{d}t} + \psi\frac{\mathrm{d}\Omega}{\mathrm{d}t} \tag{4}$$

$$\frac{\mathrm{d}\psi}{\mathrm{d}t} = \frac{1}{2}\cos(i/2)\cos(\Omega)\frac{\mathrm{d}i}{\mathrm{d}t} - \zeta\frac{\mathrm{d}\Omega}{\mathrm{d}t} \tag{5}$$

$$\frac{\mathrm{d}\lambda}{\mathrm{d}t} = \frac{\mathrm{d}f}{\mathrm{d}t} + \frac{\mathrm{d}\omega}{\mathrm{d}t} + \frac{\mathrm{d}\Omega}{\mathrm{d}t} \tag{6}$$

Recalling the well-known Gaussian variational equations for the classical elements $(a, e, i, \Omega, \omega, f)$ [17]:

$$\frac{\mathrm{d}a}{\mathrm{d}t} = \frac{2a^2}{h}\left(e\ \sin f a_r + \frac{p}{r}a_i\right) \tag{7}$$

$$\frac{\mathrm{d}e}{\mathrm{d}t} = \frac{1}{h}(p\ \sin f a_r + [(p+r)\cos f + re]a_i) \tag{8}$$

$$\frac{\mathrm{d}i}{\mathrm{d}t} = \frac{r\cos\theta}{h}a_c \tag{9}$$

$$\frac{\mathrm{d}\Omega}{\mathrm{d}t} = \frac{r\sin\theta}{h\sin i}a_c \tag{10}$$

$$\frac{\mathrm{d}\omega}{\mathrm{d}t} = \frac{1}{he}[-p\ \cos f a_r - (p+r)\sin f a_i] - \frac{r\sin\theta\cos i}{h\sin i}a_c \tag{11}$$

$$\frac{\mathrm{d}f}{\mathrm{d}t} = \frac{h}{r^2} + \frac{1}{he}[p\ \cos f a_r - (p+r)\sin f a_i] \tag{12}$$

wherein $\boldsymbol{a}_d \equiv a_r\hat{\boldsymbol{o}}_r + a_i\hat{\boldsymbol{o}}_i + a_c\hat{\boldsymbol{o}}_c$ denotes the nonconservative disturbing acceleration expressed in the local radial ($\hat{\boldsymbol{o}}_r$), in-track ($\hat{\boldsymbol{o}}_i$), and cross-track ($\hat{\boldsymbol{o}}_c$) frame of reference (i.e., the RIC frame) and the true latitude $\theta = \omega + f$. As the semi-major axis a is included in the nonsingular element set, transformation of Eq. (7) provides the first variational equation. Noting that $e\ \sin f = \eta\ \sin\lambda - \xi\ \cos\lambda$, the rate of change of the perturbed semi-major axis is rewritten as

$$\frac{\mathrm{d}a}{\mathrm{d}t} = \frac{2a^2}{h}\left[(\eta\ \sin\lambda - \xi\ \cos\lambda)a_r + \frac{p}{r}a_i\right] \tag{13}$$

where h and p denote the specific angular momentum and semi-latus rectum, respectively, and the orbit radius r is given by

$$r = \frac{a(1-\xi^2-\eta^2)}{1+\eta\ \cos\lambda + \xi\ \sin\lambda} \tag{14}$$

Substituting Eqs. (8), (10), and (11) into Eq. (2), the rate of change of the element ξ is

$$\begin{aligned}\frac{\mathrm{d}\xi}{\mathrm{d}t} = \frac{1}{h}\Bigg(&-p\ \cos\lambda a_r + [(p+r)\sin\lambda + r\xi]a_i\\ &- r\eta\left[\frac{\zeta\ \cos\lambda - \psi\ \sin\lambda}{\sqrt{1-\zeta^2-\psi^2}}\right]a_c\Bigg)\end{aligned} \tag{15}$$

where the identities $\sin(i/2)\sin\theta = \psi\ \sin\lambda - \zeta\ \cos\lambda$ and $\cos(i/2) = \sqrt{1-\zeta^2-\psi^2}$ have been employed in the nontrivial simplification. Similarly, it can be shown that the rate of change of η is

$$\begin{aligned}\frac{\mathrm{d}\eta}{\mathrm{d}t} = \frac{1}{h}\Bigg(&p\ \sin\lambda a_r + [(p+r)\cos\lambda + r\eta]a_i\\ &+ r\xi\left[\frac{\zeta\ \cos\lambda - \psi\ \sin\lambda}{\sqrt{1-\zeta^2-\psi^2}}\right]a_c\Bigg)\end{aligned} \tag{16}$$

The parameters ξ and η contain the eccentricity and the Euler angles ω and Ω, and thus may be perturbed by radial, in-track, and cross-track accelerations simultaneously. Substituting Eqs. (9) and (10) into Eq. (4), the rate of change of the parameter ζ is expressed as

$$\frac{\mathrm{d}\zeta}{\mathrm{d}t} = \frac{r}{2h\ \cos(i/2)}[\sin\theta\ \cos\Omega + \cos^2(i/2)\cos\theta\ \sin\Omega]a_c \tag{17}$$

Implementing $\cos^2(i/2) = 1 - \sin^2(i/2)$ and the expression $\sin(i/2)\cos\theta = \psi\ \cos\lambda + \zeta\ \sin\lambda$, and recalling from trigonometry that $\sin\theta\ \cos\Omega + \cos\theta\ \sin\Omega = \sin(\theta+\Omega) = \sin\lambda$, this rate becomes

$$\frac{\mathrm{d}\zeta}{\mathrm{d}t} = \frac{r}{2h\sqrt{1-\zeta^2-\psi^2}}[(1-\zeta^2)\sin\lambda - \zeta\psi\ \cos\lambda]a_c \tag{18}$$

Equivalently, the rate of change of the analogous element ψ can be converted into the following:

$$\frac{\mathrm{d}\psi}{\mathrm{d}t} = \frac{r}{2h\sqrt{1-\zeta^2-\psi^2}}[(1-\psi^2)\cos\lambda - \zeta\psi\ \sin\lambda]a_c \tag{19}$$

The parameters ζ and ψ contain the Euler angles i and Ω, and are only influenced by cross-track accelerations. Lastly, the rate of change of the longitude parameter λ in Eq. (6) is transformed:

$$\frac{\mathrm{d}\lambda}{\mathrm{d}t} = \frac{h}{r^2} - \frac{r}{h}\left[\frac{\zeta\cos\lambda - \psi\sin\lambda}{\sqrt{1-\zeta^2-\psi^2}}\right]a_c \tag{20}$$

Note that a perturbed variation in the longitude parameter λ may only be induced with cross-track accelerations. Development of the Gaussian variational equations for the nonsingular element set is complete; this formulation quantifies sensitivities of the elements to nonconservative disturbances, and is summarized for reference:

$$\begin{aligned}
\frac{\mathrm{d}a}{\mathrm{d}t} &= \frac{2a^2}{h}\left[(\eta\sin\lambda - \xi\cos\lambda)a_r + \frac{p}{r}a_i\right]\\
\frac{\mathrm{d}\xi}{\mathrm{d}t} &= \frac{1}{h}\left(-p\cos\lambda a_r + [(p+r)\sin\lambda + r\xi]a_i\right.\\
&\quad \left. - r\eta\left[\frac{\zeta\cos\lambda - \psi\sin\lambda}{\sqrt{1-\zeta^2-\psi^2}}\right]a_c\right)\\
\frac{\mathrm{d}\eta}{\mathrm{d}t} &= \frac{1}{h}\left(p\sin\lambda a_r + [(p+r)\cos\lambda + r\eta]a_i\right.\\
&\quad \left. + r\xi\left[\frac{\zeta\cos\lambda - \psi\sin\lambda}{\sqrt{1-\zeta^2-\psi^2}}\right]a_c\right)\\
\frac{\mathrm{d}\zeta}{\mathrm{d}t} &= \frac{r}{2h\sqrt{1-\zeta^2-\psi^2}}[(1-\zeta^2)\sin\lambda - \zeta\psi\cos\lambda]a_c\\
\frac{\mathrm{d}\psi}{\mathrm{d}t} &= \frac{r}{2h\sqrt{1-\zeta^2-\psi^2}}[(1-\psi^2)\cos\lambda - \zeta\psi\sin\lambda]a_c\\
\frac{\mathrm{d}\lambda}{\mathrm{d}t} &= \frac{h}{r^2} - \frac{r}{h}\left[\frac{\zeta\cos\lambda - \psi\sin\lambda}{\sqrt{1-\zeta^2-\psi^2}}\right]a_c
\end{aligned} \tag{21}$$

These variational equations are nonsingular for circular and equatorial orbits, and furthermore, as this formulation eliminates the numerical difficulties arising in the variational equations in classical elements for near-circular orbits, this nonsingular set is advantageous for chief motions in the GEO regime. Equation (21) is convenient for quantifying the effects of a control thrust on each of the nonsingular elements, and is thus implemented as a basis for the impulsive control strategy.

III. Development of Impulsive Feedback Control Law

An N-impulse feedback technique is developed for controlling nonsingular element differences between the chief and deputy spacecraft at discrete positions in orbit with predetermined impulsive maneuvers, rather than with continuous thrust. Writing Eq. (21) with an impulsive $\Delta\boldsymbol{v}$ thrust in the orbit frame, and considering only the perturbed response of the longitude parameter rate $\dot{\lambda}$:

$$\Delta a = \frac{2a^2}{h}\left[(\eta\sin\lambda - \xi\cos\lambda)\Delta v_r + \frac{p}{r}\Delta v_i\right] \tag{22}$$

$$\begin{aligned}
\Delta\xi = \frac{1}{h}\left(-p\cos\lambda\Delta v_r + [(p+r)\sin\lambda + r\xi]\Delta v_i\right.\\
\left. - r\eta\left[\frac{\zeta\cos\lambda - \psi\sin\lambda}{\sqrt{1-\zeta^2-\psi^2}}\right]\Delta v_c\right)
\end{aligned} \tag{23}$$

$$\begin{aligned}
\Delta\eta = \frac{1}{h}\left(p\sin\lambda\Delta v_r + [(p+r)\cos\lambda + r\eta]\Delta v_i\right.\\
\left. + r\xi\left[\frac{\zeta\cos\lambda - \psi\sin\lambda}{\sqrt{1-\zeta^2-\psi^2}}\right]\Delta v_c\right)
\end{aligned} \tag{24}$$

$$\Delta\zeta = \frac{r}{2h\sqrt{1-\zeta^2-\psi^2}}[(1-\zeta^2)\sin\lambda - \zeta\psi\cos\lambda]\Delta v_c \tag{25}$$

$$\Delta\psi = \frac{r}{2h\sqrt{1-\zeta^2-\psi^2}}[(1-\psi^2)\cos\lambda - \zeta\psi\sin\lambda]\Delta v_c \tag{26}$$

$$\Delta\lambda = -\frac{r}{h}\left[\frac{\zeta\cos\lambda - \psi\sin\lambda}{\sqrt{1-\zeta^2-\psi^2}}\right]\Delta v_c \tag{27}$$

Note that Eqs. (25) and (26) can be rewritten in the form

$$\Delta\zeta = \frac{r\sin\lambda}{2h}\sqrt{1-\zeta^2-\psi^2}\Delta v_c + \frac{\psi}{2}\Delta\lambda \tag{28}$$

$$\Delta\psi = \frac{r\cos\lambda}{2h}\sqrt{1-\zeta^2-\psi^2}\Delta v_c - \frac{\zeta}{2}\Delta\lambda \tag{29}$$

Corrections in the longitude parameter λ are linearly related to corrections in the (ζ,ψ) elements, and as a result, errors in the longitude parameter, and consequently the true anomaly angle, cannot be independently controlled with a feedback scheme constructed around this set of elements. Note, however, that the true anomaly can be corrected by performing a phasing maneuver in which the semi-major axis is raised or lowered temporarily, to yield relative drift for the required phase shift.

An N-impulse approach is implemented to alleviate difficulties arising in the complexity of the nonsingular variational equations provided in Eq. (21). Schaub and Alfriend [1] develop an impulsive firing scheme in which subsets of the full Keplerian element set are corrected simultaneously, by studying the Gaussian variational equations to find ideal times at which to execute the corrective maneuvers. However, with this nonsingular element set, innate complexity of the variational equations renders an analogous analytical solution challenging to determine. Thus, rather than seeking an analytical solution for the desired nonsingular element corrections, a swift numerical technique that determines the ideal burn locations for achieving these relative orbit corrections is sought here.

A. Formulation of Control Strategy

In a manner analogous to that used in [1], element errors $\Delta\boldsymbol{e} \equiv (\Delta a, \Delta\xi, \Delta\eta, \Delta\zeta, \Delta\psi)^T$ are held fixed at the beginning of the time frame of correction. An N-impulse sequence is then implemented over the current revolution, where the burns are executed at uniform increments in true anomaly, such that $N = 360\ \mathrm{deg}/f_{\Delta v}$, wherein $f_{\Delta v}$ is the specified true anomaly increment expressed in degrees per burn (in this sense, the N-impulse sequence may be treated as a discretization of a continuous, low-thrust control effort). For the jth impulse $\Delta\boldsymbol{v}_j \equiv (\Delta v_r^j, \Delta v_i^j, \Delta v_c^j)^T$, the contribution to the desired nonsingular element corrections becomes

$$\Delta a_j = \frac{2a^2}{h}\left[(\eta\sin\lambda_j - \xi\cos\lambda_j)\Delta v_r^j + \frac{p}{r_j}\Delta v_i^j\right] \tag{30}$$

$$\begin{aligned}
\Delta\xi_j = \frac{1}{h}\left(-p\cos\lambda_j\Delta v_r^j + [(p+r_j)\sin\lambda_j + r_j\xi]\Delta v_i^j\right.\\
\left. - r_j\eta\left[\frac{\zeta\cos\lambda_j - \psi\sin\lambda_j}{\sqrt{1-\zeta^2-\psi^2}}\right]\Delta v_c^j\right)
\end{aligned} \tag{31}$$

$$\begin{aligned}
\Delta\eta_j = \frac{1}{h}\left(p\sin\lambda_j\Delta v_r^j + [(p+r_j)\cos\lambda_j + r_j\eta]\Delta v_i^j\right.\\
\left. + r_j\xi\left[\frac{\zeta\cos\lambda_j - \psi\sin\lambda_j}{\sqrt{1-\zeta^2-\psi^2}}\right]\Delta v_c^j\right)
\end{aligned} \tag{32}$$

$$\Delta\zeta_j = \frac{r_j}{2h\sqrt{1-\zeta^2-\psi^2}}[(1-\zeta^2)\sin\lambda_j - \zeta\psi\cos\lambda_j]\Delta v_c^j \quad (33)$$

$$\Delta\psi_j = \frac{r_j}{2h\sqrt{1-\zeta^2-\psi^2}}[(1-\psi^2)\cos\lambda_j - \zeta\psi\sin\lambda_j]\Delta v_c^j \quad (34)$$

wherein the subscript j denotes conditions at the execution of the jth burn. Parameters without this subscript, including the nonsingular elements of the maneuvering spacecraft, are fixed at the beginning of the correction sequence in Eqs. (30–34). As this piecewise constant assumption neglects the influence of subsequent impulses on these elements, this feedback strategy is designed to significantly reduce — not completely eliminate — errors in nonsingular element differences over a single revolution. Multiple correction orbits may be readily employed to fully nullify these errors if desired, by fixing the residual errors at the beginning of each correction orbit, and executing an updated N-impulse maneuver sequence for the current revolution, which is computed as follows.

For compactness, corrections to the nonsingular elements due to the jth burn are rewritten as

$$\Delta a_j = \Delta a_j^r \Delta v_r^j + \Delta a_j^i \Delta v_i^j \quad (35)$$

$$\Delta\xi_j = \Delta\xi_j^r \Delta v_r^j + \Delta\xi_j^i \Delta v_i^j + \Delta\xi_j^c \Delta v_c^j \quad (36)$$

$$\Delta\eta_j = \Delta\eta_j^r \Delta v_r^j + \Delta\eta_j^i \Delta v_i^j + \Delta\eta_j^c \Delta v_c^j \quad (37)$$

$$\Delta\zeta_j = \Delta\zeta_j^c \Delta v_c^j \quad (38)$$

$$\Delta\psi_j = \Delta\psi_j^c \Delta v_c^j \quad (39)$$

where the following definitions have been used:

$$\Delta a_j^r \equiv \frac{2a^2}{h}(\eta\sin\lambda_j - \xi\cos\lambda_j) \quad (40)$$

$$\Delta a_j^i \equiv \frac{2a^2 p}{h r_j} \quad (41)$$

$$\Delta\xi_j^r \equiv -\frac{p}{h}\cos\lambda_j \quad (42)$$

$$\Delta\xi_j^i \equiv \frac{1}{h}[(p+r_j)\sin\lambda_j + r_j\xi] \quad (43)$$

$$\Delta\xi_j^c \equiv \frac{r_j\eta}{h}\left[\frac{\zeta\cos\lambda_j\psi\sin\lambda_j}{\sqrt{1-\zeta^2-\psi^2}}\right] \quad (44)$$

$$\Delta\eta_j^r \equiv \frac{p}{h}\sin\lambda_j \quad (45)$$

$$\Delta\eta_j^i \equiv \frac{1}{h}[(p+r_j)\cos\lambda_j + r_j\eta] \quad (46)$$

$$\Delta\eta_j^c \equiv \frac{r_j\xi}{h}\left[\frac{\zeta\cos\lambda_j - \psi\sin\lambda_j}{\sqrt{1-\zeta^2-\psi^2}}\right] \quad (47)$$

$$\Delta\zeta_j^c \equiv \frac{r_j}{2h\sqrt{1-\zeta^2-\psi^2}}[(1-\zeta^2)\sin\lambda_j - \zeta\psi\cos\lambda_j] \quad (48)$$

$$\Delta\psi_j^c \equiv \frac{r_j}{2h\sqrt{1-\zeta^2-\psi^2}}[(1-\psi^2)\cos\lambda_j - \zeta\psi\sin\lambda_j] \quad (49)$$

The total corrections $\Delta\boldsymbol{e} = \sum_{j=1}^{N}\Delta\boldsymbol{e}_j$ due to the N impulses executed in the correction orbit are

$$\begin{pmatrix}\Delta a\\ \Delta\xi\\ \Delta\eta\\ \Delta\zeta\\ \Delta\psi\end{pmatrix} = \begin{pmatrix}\Delta a_1^r & \Delta a_1^i & 0 & \dots & \Delta a_j^r & \Delta a_j^i & 0 & \dots & \Delta a_N^r & \Delta a_N^i & 0\\ \Delta\xi_1^r & \Delta\xi_1^i & \Delta\xi_1^c & \dots & \Delta\xi_j^r & \Delta\xi_j^i & \Delta\xi_j^c & \dots & \Delta\xi_N^r & \Delta\xi_N^i & \Delta\xi_N^c\\ \Delta\eta_1^r & \Delta\eta_1^i & \Delta\eta_1^c & \dots & \Delta\eta_j^r & \Delta\eta_j^i & \Delta\eta_j^c & \dots & \Delta\eta_N^r & \Delta\eta_N^i & \Delta\eta_N^c\\ 0 & 0 & \Delta\zeta_1^c & \dots & 0 & 0 & \Delta\zeta_j^c & \dots & 0 & 0 & \Delta\zeta_N^c\\ 0 & 0 & \Delta\psi_1^c & \dots & 0 & 0 & \Delta\psi_j^c & \dots & 0 & 0 & \Delta\psi_N^c\end{pmatrix}\begin{pmatrix}\Delta v_r^1\\ \Delta v_i^1\\ \Delta v_c^1\\ \vdots\\ \Delta v_r^j\\ \Delta v_i^j\\ \Delta v_c^j\\ \vdots\\ \Delta v_r^N\\ \Delta v_i^N\\ \Delta v_c^N\end{pmatrix} \quad (50)$$

which may be written compactly in the linear form

$$\Delta\boldsymbol{e} = [B(\boldsymbol{e}_j)]\Delta\boldsymbol{v}_{\text{seq}} \quad (51)$$

where the total corrections $\Delta\boldsymbol{e}$ are the specified errors in the nonsingular element set of the deputy. The objective of this feedback strategy is to compute the N-impulse burn sequence $\Delta\boldsymbol{v}_{\text{seq}}$ that satisfies Eq. (51) and simultaneously minimizes the fuel cost required to perform the corrective sequence, such that the desired nonsingular element differences can be efficiently achieved. Because nonsingular element differences between the chief and deputy spacecraft are nonintuitive to visualize, the first-order mapping from these differences to the relative state in the well-known Hill frame is presented in Appendix A. Note that $[B(\boldsymbol{e}_j)]$ is of dimension $5\times 3N$ and cannot

be inverted. To obtain the fuel-optimal N-impulse sequence, the following nonlinear programming (NLP) problem governing this feedback control strategy must be solved:

$$\underset{\Delta v_{\text{seq}}}{\text{minimize}}\ J \equiv \sum_{j=1}^{N} \|\Delta v_j\| = \sum_{j=1}^{N} \sqrt{\Delta v_r^j \Delta v_r^j + \Delta v_i^j \Delta v_i^j + \Delta v_c^j \Delta v_c^j}$$

$$\text{subject to } \boldsymbol{G} \equiv [B(\boldsymbol{e}_j)]\Delta \boldsymbol{v}_{\text{seq}} - \Delta \boldsymbol{e} = \boldsymbol{0} \tag{52}$$

The minimum-norm inverse of $[B(\boldsymbol{e}_j)]$ is inappropriate in this situation, as this formulation will minimize $\|\Delta \boldsymbol{v}_{\text{seq}}\|$, and not the desired cost function given in Eq. (52): we seek to minimize the sum of the individual impulse magnitudes, not the vector norm of the entire impulse sequence. The solution to Eq. (52) provides the minimum-fuel N-impulse sequence that attenuates the fixed errors specified in these nonsingular elements. The gradient of the objective function follows as

$$\frac{\partial J}{\partial \Delta \boldsymbol{v}_{\text{seq}}} = \left(\frac{\Delta \boldsymbol{v}_1^T}{\|\Delta \boldsymbol{v}_1\|} \quad \cdots \quad \frac{\Delta \boldsymbol{v}_j^T}{\|\Delta \boldsymbol{v}_j\|} \quad \cdots \quad \frac{\Delta \boldsymbol{v}_N^T}{\|\Delta \boldsymbol{v}_N\|} \right)^T \tag{53}$$

The Jacobian of the equality constraints follows from Eq. (52):

$$\frac{\partial \boldsymbol{G}}{\partial \Delta \boldsymbol{v}_{\text{seq}}} = [B(\boldsymbol{e}_j)] \tag{54}$$

For this study, MATLAB's constrained minimization solver *fmincon* is used with the active-set algorithm to obtain a solution to the NLP problem posed in Eq. (52). At the beginning of the correction orbit, the nonsingular element errors $\Delta \boldsymbol{e}$ are fixed, and $[B(\boldsymbol{e}_j)]$ is precomputed with the given longitude increments

$$\lambda_j = f_0 + j f_{\Delta v} + \omega + \Omega, \qquad j = 1, 2, \ldots, N \tag{55}$$

wherein f_0 is the true anomaly at the beginning of the correction orbit. The fuel-optimal maneuver sequence $\Delta \boldsymbol{v}_{\text{seq}}$ is then achieved by solving Eq. (52) with *fmincon*, and is executed during the current revolution to correct the element errors $\Delta \boldsymbol{e}$. For the example cases considered, an initial guess of $\Delta \boldsymbol{v}_{\text{seq}} \equiv (\Delta \boldsymbol{v}_1, \ldots, \Delta \boldsymbol{v}_j, \ldots, \Delta \boldsymbol{v}_N)^T$ where $\Delta \boldsymbol{v}_j = (1, 1, 1)^T$ m/s $\forall\ j = 1, 2, \ldots, N$ is used for initializing the *fmincon* optimizer. As this initial guess is not guaranteed to be suitable for general situations, simulations show that using a small, nonzero $\Delta \boldsymbol{v}_j\ \forall\ j$ can assist in improving convergence if the optimization algorithm fails to determine a solution for a desired N. For nonintuitive corrections that present challenging convergence issues, a continuation technique can be harnessed, in which solutions for coarser true anomaly increments are used to seed the optimizer for successively finer increments, until a solution for the desired burn resolution is achieved. The optimizer does not vary N or the impulse locations in this formulation — only the burn magnitudes are varied. This strategy uses solutions for small N as a first guess of solutions for successively larger N to improve convergence. Dependence of the optimizer solution on the initial guess for the maneuver sequence $\Delta \boldsymbol{v}_{\text{seq}}$ and the specified number of impulses N is discussed in Sec. III.B.

B. Examples of Control Strategy

Two example cases are presented to validate the N-impulse control developed in Sec. III.A. For simplicity, the deputy and chief are assumed to begin at the same location on equivalent orbits (thus, the following examples simulate a deployment sequence in which the deputy is maneuvered to a different orbit relative to the chief). Because nonsingular element sets are less intuitive to visualize, Keplerian orbit element differences are specified for the test examples; the classical differences are converted into nonsingular differences required by this N-impulse control technique. Thus, the nonsingular element set is used here as an under-the-hood mechanism for avoiding singularities in the variational equations for the classical elements. As the inertial frame (i.e., J2000) is used for control implementation, the optimal maneuver sequence must be rotated from the local orbit frame to the inertial frame during numerical integration and impulse execution.

Table 1 Initial and desired conditions for Example 1

Element	Deputy	Desired	$\Delta \boldsymbol{e}_{\text{coe}}$
a	42164 km	42164 km	0 km
e	0.0001	0.0001	0
i	10 deg	10.001 deg	0.001 deg
Ω	0 deg	0 deg	0 deg
ω	0 deg	0 deg	0 deg
f_0	0 deg	N/A	N/A

Furthermore, the impulse sequences are executed under both two-body forcing and a perturbed force model that includes 4×4 EGM-96 gravitation, luni-solar perturbations, and the solar radiation pressure (SRP) perturbation. Schaub and Jasper [18] indicate that an area-to-mass ratio of 0.04 m^2/kg is representative for geostationary satellites; thus, this value is implemented for computing the cannonball SRP acceleration [19] modeled in these example simulations. Because this control strategy is formulated under the assumption that the two-body dynamics are perturbed only by the applied impulses, including this set of representative environmental disturbances illustrates that this strategy corrects relative orbit errors, even under more representative forcing that is unmodeled in the two-body framework of this technique.

1. *Example 1: Inclination Change*

The first example examines the case of an inclination change, in which it is known from basic orbit mechanics that the most efficient location for a plane change is at the equator crossing [17]. The initial deputy and desired conditions simulated for this example are provided in Table 1. Impulses are specified to occur every $f_{\Delta v} = 10$ deg for one revolution, such that $N = 36$ for this example. The value of the true anomaly increment — and subsequently the number of impulses N — is selected arbitrarily in these example simulations, to illustrate controller validity and performance for various NLP optimizer configurations. The optimal maneuver sequence is shown in Fig. 1, and the error history of the nonsingular elements during execution of this sequence is illustrated in Fig. 2. As anticipated, the radial and in-track burns are nearly zero at all burn locations, whereas the cross-track burn spikes at the positions of the descending and ascending nodes to raise the orbit plane. The total fuel cost for this burn sequence is $\Delta v_{\text{cost}} = 5.379$ cm/s, slightly larger than the single-impulse solution [20]

$$\Delta v_{1\text{-burn}} = 2 v_n \sin \frac{\Delta i}{2} = 5.367 \text{ cm/s} \tag{56}$$

where v_n is the velocity magnitude at the node and $\Delta i = 0.001$ deg is the specified inclination change. Thus, the control strategy approximately replicates the optimal single-impulse solution for this example. Because the control strategy is executed over a single revolution, the total Δv_{cost} is equivalent for both the two-body and perturbed forcing cases.

2. *Example 2: General Orbit Transfer*

The second example illustrates the case of a general orbit transfer, in which errors in the elements $(a, e, i, \Omega, \omega)$ are present and require correction with a multi-revolution maneuver sequence. The initial deputy and desired conditions simulated for this example are provided in Table 2. Impulses are specified to occur every $f_{\Delta v} = 5$ deg for three revolutions, such that $N = 72$ burns per correction orbit for this example. The optimal maneuver sequence is illustrated in Fig. 3, and the error history of the nonsingular elements during execution of this sequence is illustrated in Fig. 4. For this solution, burn magnitudes in all three orbit frame directions sharply increase at the ascending and descending nodes during the first revolution, nullifying errors in the (η, ψ) elements. The semi-major axis is

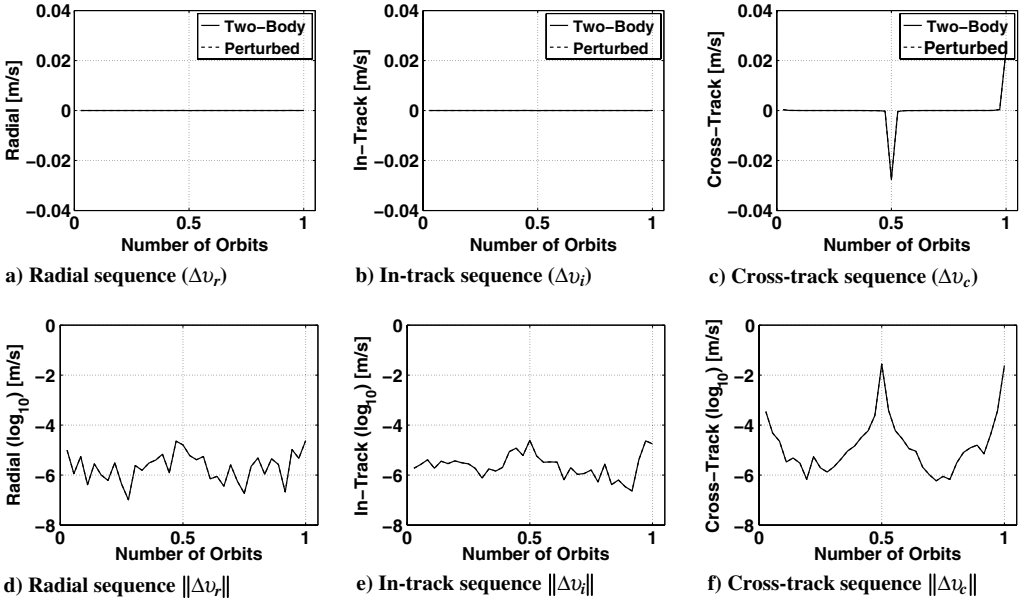

a) Radial sequence (Δv_r) b) In-track sequence (Δv_i) c) Cross-track sequence (Δv_c)

d) Radial sequence $\|\Delta v_r\|$ e) In-track sequence $\|\Delta v_i\|$ f) Cross-track sequence $\|\Delta v_c\|$

Fig. 1 Fuel-optimal burn sequence determined by feedback control strategy for Example 1.

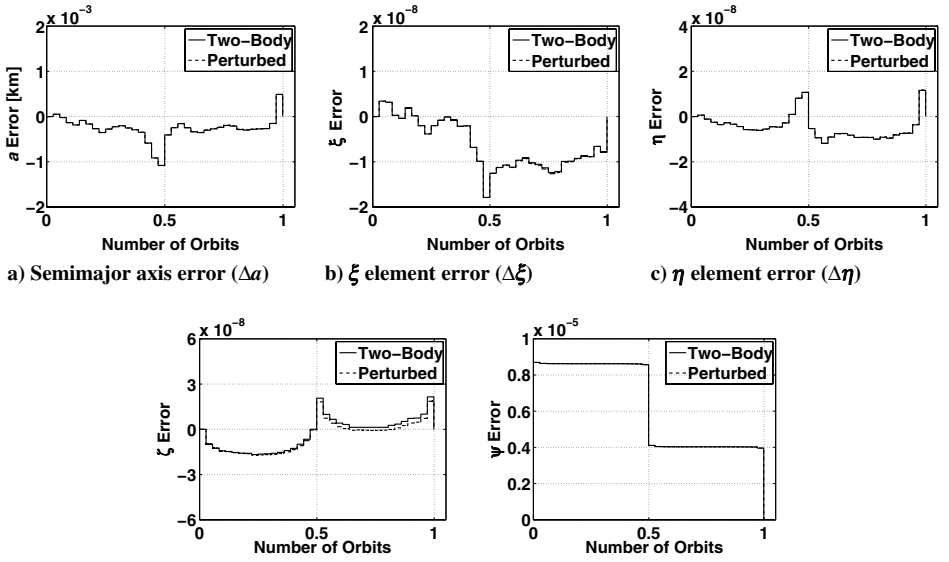

a) Semimajor axis error (Δa) b) ξ element error ($\Delta\xi$) c) η element error ($\Delta\eta$)

d) ζ element error ($\Delta\zeta$) e) ψ element error ($\Delta\psi$)

Fig. 2 Error history of nonsingular elements during burn sequence execution for Example 1.

corrected after the second revolution, and errors in the (ξ, ζ) elements are mitigated following the complete three revolution sequence. Note that the control performs nearly equivalently under both two-body and perturbed forcing — the fuel cost for this maneuver sequence is approximately $\Delta v_{\text{cost}} = 17.66$ m/s in both the two-body and perturbed cases.

Relative orbit geometry during execution of the maneuver sequence for Example 2 is illustrated in Fig. 5. Impulse locations and the relative trajectory of the deputy in the Hill frame of the chief are shown in Fig. 5a, and the final orbit as predicted by the full nonlinear mapping (i.e., inertial differencing of the chief and deputy trajectories) and the linear mapping given in Appendix A over one revolution is illustrated in Fig. 5b. This linear mapping therefore provides a sufficient and computationally efficient means of predicting relative orbit geometry in the Hill frame with a given set of nonsingular element differences between the chief and deputy spacecraft.

It is interesting to highlight the sensitivity of the optimizer solution for this particular example to the initial guess for the maneuver sequence $\Delta \boldsymbol{v}_{\text{seq}}$ and the number of impulses N. Table 3 lists the total fuel cost output by the optimization routine for various initial maneuver sequences and true anomaly increments. As indicated by the results on the left of Table 3, the optimizer converges upon neighboring local minima with similar fuel costs, even as the initial guess of $\Delta \boldsymbol{v}_j = (1, 1, 1)^T$ m/s $\forall\ j = 1, 2, \ldots, N$ is varied by a factor of 10 — thus, for this example, this control algorithm is

Table 2 Initial and desired conditions for Example 2

Element	Deputy	Desired	Δe_{coe}
a	42164 km	42164.1 km	0.1 km
e	0.2	0.21	0.01
i	10 deg	10.1 deg	0.1 deg
Ω	0 deg	0.1 deg	0.1 deg
ω	0 deg	0.1 deg	0.1 deg
f_0	0 deg	N/A	N/A

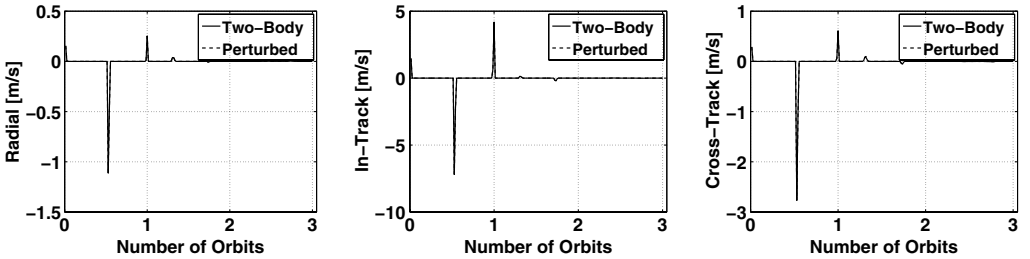

a) Radial sequence (Δv_r) b) In-track sequence (Δv_i) c) Cross-track sequence (Δv_c)

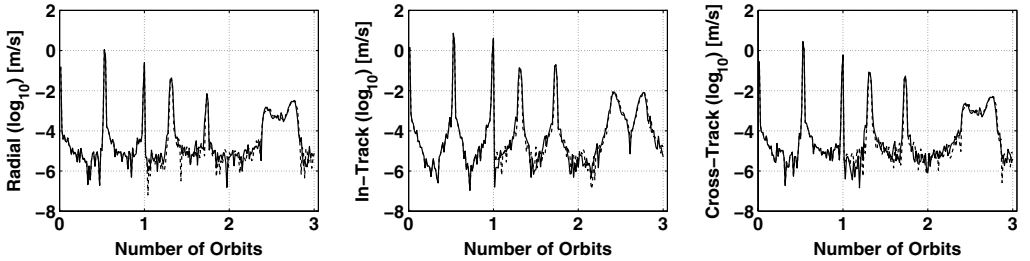

d) Radial sequence $\|\Delta v_r\|$ e) In-track sequence $\|\Delta v_i\|$ f) Cross-track sequence $\|\Delta v_c\|$

Fig. 3 Fuel-optimal burn sequence determined by feedback control strategy for Example 2.

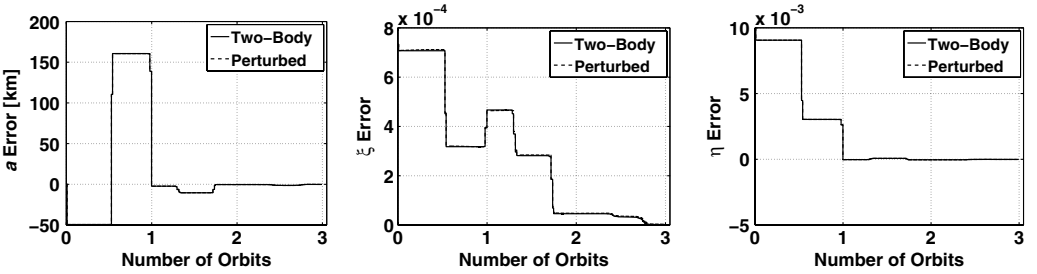

a) Semimajor axis error (Δa) b) ξ element error ($\Delta\xi$) c) η element error ($\Delta\eta$)

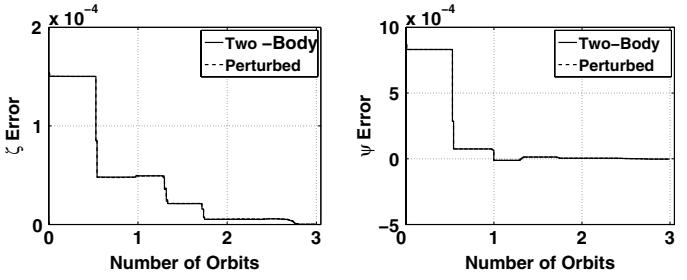

d) ζ element error ($\Delta\zeta$) e) ψ element error ($\Delta\psi$)

Fig. 4 Error history of nonsingular elements during burn sequence execution for Example 2.

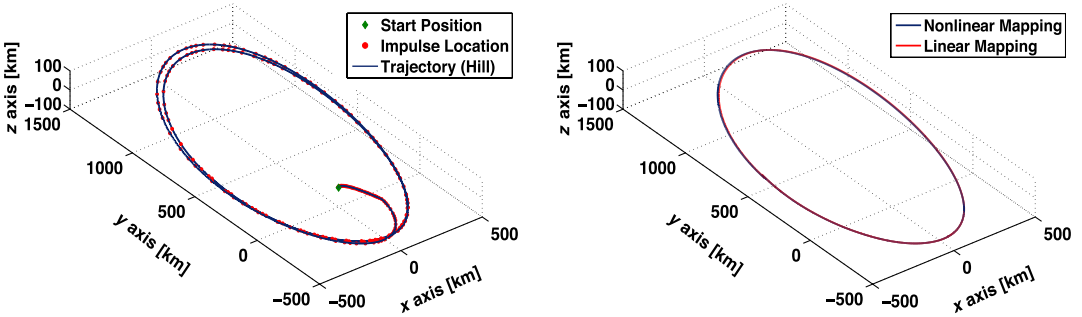

a) Impulse locations on relative orbit for Example 2 b) Final relative orbit as predicted by two mappings

Fig. 5 Relative orbit geometry in Hill frame during burn sequence execution for Example 2.

Table 3 Sensitivity of solution to initial guess and number of impulses

Initial $\Delta \boldsymbol{v}_{\text{seq}}$ Guess $[f_{\Delta v} = 5$ deg]	Δv_{cost} [m/s]	${}^{j}f_{\Delta v}(N)$ $[\Delta v^{j}_{r,i,c} = 1$ m/s]	Δv_{cost} [m/s]
$\Delta v^{j}_{r,i,c} = 0.1$ m/s	17.706	90 deg (4)	19.427
$\Delta v^{j}_{r,i,c} = 1$ m/s	17.664	45 deg (8)	18.858
$\Delta v^{j}_{r,i,c} = 2$ m/s	17.682	30 deg (12)	20.009
$\Delta v^{j}_{r,i,c} = 5$ m/s	17.715	10 deg (36)	17.987
$\Delta v^{j}_{r,i,c} = 10$ m/s	17.777	5 deg (72)	17.664

sufficiently robust to a sizable range of initial conditions input to the optimizer. Furthermore, the results on the right of Table 3 highlight that, in general, the cost of the control solution decreases with increasing N. This is an intuitive result, as a larger number of burns over a single revolution better approximates a continuous thrusting effort, such that optimal impulse locations can be more readily detected with this algorithm. As convergence is increasingly challenging with larger N, we emphasize the continuation technique discussed in Sec. III.A for improvements in performance.

IV. Conclusions

An N-impulse feedback control technique is developed to correct errors in a set of nonsingular element differences between a chief and deputy spacecraft. The Gaussian variational equations for this nonsingular set are derived to construct a basis for this N-impulse feedback control law. Using this technique, a near-optimal burn sequence may be rapidly determined to generate an estimate of appropriate initial conditions for more complex, nonlinear optimization algorithms. By specifying impulses to occur at defined increments in true anomaly, this technique detects fuel-optimal burn locations for general transfers in which optimal burn locations are unknown, such that ideal initial conditions for a nonlinear optimizer seeking a two- or three-burn solution are discerned. Further, because the nonsingular element set harnessed in this study is well-defined for zero eccentricity and inclination, this control strategy is especially convenient for GEO orbits with these characteristics.

Appendix: Development of Forward Linear Mapping

Derivation of the linear mapping from differences in the nonsingular element set in Eq. (1) to the Hill frame Cartesian state of the deputy is performed by transforming the variational terms in the linear mapping developed in [21]. The noninertial Hill frame of reference is centered at the chief spacecraft and implements rotating axes that point in the local radial ($\hat{\boldsymbol{o}}_r$), in-track ($\hat{\boldsymbol{o}}_i$), and cross-track ($\hat{\boldsymbol{o}}_c$) directions of the chief spacecraft [17]. For reference, the Hill frame description of relative motion is illustrated in Fig. 6. The linear mapping

$$\boldsymbol{X} = [A(\boldsymbol{e}_c)]\delta\boldsymbol{e} \tag{A1}$$

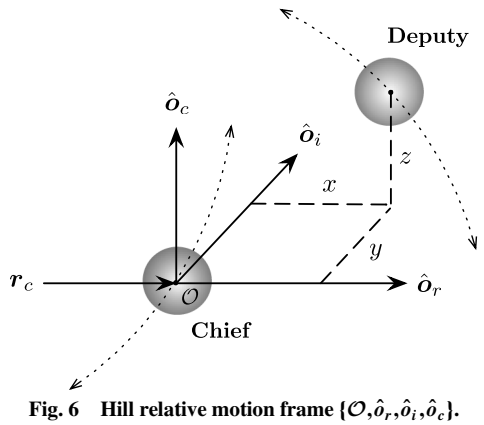

Fig. 6 Hill relative motion frame $\{\mathcal{O},\hat{\boldsymbol{o}}_r,\hat{\boldsymbol{o}}_i,\hat{\boldsymbol{o}}_c\}$.

where $\boldsymbol{X} = (x, y, z, \dot{x}, \dot{y}, \dot{z})^T$ is the Hill frame state and $\delta\boldsymbol{e}$ is the set of element differences, is thus converted into a form consistent with the description

$$\delta\boldsymbol{e} = \boldsymbol{e}_d - \boldsymbol{e}_c \equiv (\delta a, \delta\xi, \delta\eta, \delta\zeta, \delta\psi, \delta\lambda)^T \tag{A2}$$

where $\boldsymbol{e}_d$ and $\boldsymbol{e}_c$ denote the elements of the deputy and chief spacecraft, respectively. The forward mapping linearizes about the chief motion – deviation from this reference must therefore be small such that this approximation remains valid in the truncation of higher-order terms beyond those of the first-order [17]. Note that although this formulation provides for perturbations, Keplerian motion is assumed, as each of the nonsingular element differences with the exception of $\delta\lambda$ is invariant in this case.

The complete linear mapping from nonsingular element differences is shown to be [22]

$$\begin{aligned}
x &= \frac{1}{\alpha}\delta a - \rho(2a\xi + r\sin\lambda)\delta\xi - \rho(2a\eta + r\cos\lambda)\delta\eta + r\nu\delta\lambda \\
y &= r(-2\psi\delta\zeta + 2\zeta\delta\psi + \delta\lambda) \\
z &= \frac{2r}{\sqrt{1-\zeta^2-\psi^2}}\{[(\psi^2-1)\cos\lambda + \zeta\psi\sin\lambda]\delta\zeta \\
&\quad - [(\zeta^2-1)\sin\lambda + \zeta\psi\cos\lambda]\delta\psi\} \\
\dot{x} &= -\frac{V_r}{2a}\delta a + (V_r a\xi - h\cos\lambda)\frac{\delta\xi}{p} + (V_r a\eta + h\sin\lambda)\frac{\delta\eta}{p} \\
&\quad + \left(\frac{1}{r} - \frac{1}{p}\right)h\delta\lambda \\
\dot{y} &= -\frac{3V_t}{2a}\delta a + (3V_t a\xi + 2h\sin\lambda)\frac{\delta\xi}{p} + (3V_t a\eta + 2h\cos\lambda)\frac{\delta\eta}{p} \\
&\quad - 2V_r\psi\delta\zeta + 2V_r\zeta\delta\psi - V_r\delta\lambda \\
\dot{z} &= \frac{2h}{p\sqrt{1-\zeta^2-\psi^2}}[(1-\psi^2)(\xi+\sin\lambda) + \zeta\psi(\eta+\cos\lambda)]\delta\zeta \\
&\quad + \frac{2h}{p\sqrt{1-\zeta^2-\psi^2}}[(1-\zeta^2)(\eta+\cos\lambda) + \zeta\psi(\xi+\sin\lambda)]\delta\psi
\end{aligned} \tag{A3}$$

These transformations satisfy the linear mapping provided in Eq. (A1) for the nonsingular set of orbital element differences given by Eq. (A2). The relative Hill frame state of the deputy can thus be expressed as a function of the chief elements $\boldsymbol{e}_c$ and the instantaneous differences $\delta\boldsymbol{e}$. Note this description is valid for Keplerian motion and general elliptic chief eccentricities [17]. Complete details for the derivation and validation of this linear mapping are presented in [22].

References

[1] Schaub, H., and Alfriend, K. T., "Impulsive Feedback Control to Establish Specific Mean Orbit Elements of Spacecraft Formations," *Journal of Guidance, Navigation, and Control*, Vol. 24, No. 4, Aug. 2001, pp. 739–745.

[2] Schaub, H., "Spacecraft Relative Orbit Geometry Description Through Orbit Element Differences," *Proceedings of the 14th U.S. National Congress of Theoretical and Applied Mechanics*, June 2002.

[3] Schaub, H., "Incorporating Secular Drifts into the Orbit Element Difference Description of Relative Orbits," *Proceedings of the 13th AAS/AIAA Space Flight Mechanics Meeting*, Univelt, Inc., San Diego, CA, Feb. 2003, pp. 239–258; also AAS Paper 2003-115.

[4] Cougnet, C., Gerber, B., and Visentin, G., "On-Orbit Servicing System Architectures for GEO and MEO Constellations," *Proceedings of the 57th International Astronautical Congress*, International Astronautical Federation, Oct. 2006.

[5] Alfriend, K. T., Lee, D., and Creamer, N., "Optimal Servicing of Geosynchronous Satellites," *Journal of Guidance, Control, and Dynamics*, Vol. 29, No. 1, 2006, pp. 203–206. doi:10.2514/1.15602

[6] Shen, H., and Tsiotras, P., "Peer-to-Peer Refueling for Circular Satellite Constellations," *Journal of Guidance, Control, and Dynamics*, Vol. 28, No. 6, 2005, pp. 1220–1230. doi:10.2514/1.9570

[7] Tombasco, J., "Orbit Estimation of Geosynchronous Objects via Ground-Based and Space-Based Optical Tracking," Ph.D. Dissertation, Univ. of Colorado at Boulder, Boulder, CO, 2011.

[8] Vadali, S. R., Schaub, H., and Alfriend, K. T., "Initial Conditions and Fuel-Optimal Control for Formation Flying Satellites," *Proceedings of the 1999 AIAA Guidance, Navigation and Control Conference*, AIAA, Reston, VA, Aug. 1999; also AIAA Paper 1999-4265.

[9] Choi, Y., Mok, S., and Bang, H., "Impulsive Formation Control Using Orbital Energy and Angular Momentum Vector," *Acta Astronautica*, Vol. 67, Nos. 5–6, 2010, pp. 613–622. doi:10.1016/j.actaastro.2010.04.008

[10] Tong, C., Shijie, X., and Songxia, W., "Relative Motion Control for Autonomous Rendezvous Based on Classical Orbit Element Differences," *Journal of Guidance, Control, and Dynamics*, Vol. 30, No. 4, July–Aug. 2007, pp. 1003–1014. doi:10.2514/1.28250

[11] Prussing, J. E., and Chiu, J. H., "Optimal Multiple-Impulse Time-Fixed Rendezvous Between Circular Orbits," *Journal of Guidance, Control, and Dynamics*, Vol. 9, No. 1, Jan. 1986, pp. 17–22. doi:10.2514/3.20060

[12] Shen, H., and Tsiotras, P., "Optimal Two-Impulse Rendezvous using Multiple-Revolution Lambert Solutions," *Journal of Guidance, Control, and Dynamics*, Vol. 26, No. 1, 2003, pp. 50–61. doi:10.2514/2.5014

[13] Smith, J. E., "Application of Optimization Techniques to the Design and Maintenance of Satellite Constellations," M.S. Thesis, Massachusetts Inst. of Technology, Cambridge, MA, June 1999.

[14] Abdelkhalik, O., and Mortari, D., "*N*-Impulse Orbit Transfer Using Genetic Algorithms," *Journal of Spacecraft and Rockets*, Vol. 44, No. 2, 2007, pp. 456–459. doi:10.2514/1.24701

[15] Nacozy, P., and Dallas, S., "The Geopotential in Nonsingular Elements," *Celestial Mechanics*, Vol. 15, No. 4, 1977, pp. 453–466. doi:10.1007/BF01228611

[16] Broucke, R. A., and Cefola, P. J., "On the Equinoctial Orbit Elements," *Celestial Mechanics*, Vol. 5, No. 3, 1972, pp. 303–310. doi:10.1007/BF01228432

[17] Schaub, H., and Junkins, J. L., *Analytical Mechanics of Space Systems*, 2nd ed., AIAA Education Series, Reston, VA, 2009, pp. 673–749.

[18] Schaub, H., and Jasper, L. E. Z., "Circular Orbit Radius Control Using Electrostatic Actuation for 2-Craft Configurations," *Proceedings of the 2011 AAS/AIAA Astrodynamics Specialist Conference*, Univelt, Inc., San Diego, CA, Aug. 2011, pp. 1479–1496; also AAS Paper 2011-498.

[19] Vallado, D., *Fundamentals of Astrodynamics and Applications*, 3rd ed., Microcosm Press, Hawthorne, CA, 2007, pp. 574–577.

[20] Curtis, H., *Orbital Mechanics for Engineering Students*, 1st ed., Elsevier Butterworth-Heinemann, Oxford, U.K., 2005, pp. 290–292.

[21] Alfriend, K. T., Schaub, H., and Gim, D. W., "Gravitational Perturbations, Nonlinearity and Circular Orbit Assumption Effects on Formation Flying Control Strategies," *2000 AAS Guidance and Control Conference Proceedings*, Univelt, Inc., San Diego, CA, Feb. 2000, pp. 139–158; also AAS Paper 2000-012.

[22] Anderson, P. V., and Schaub, H., "Impulsive Feedback Control of Nonsingular Elements in the Geostationary Regime," *Proceedings of the 2012 AIAA/AAS Astrodynamics Specialist Conference*, Curran Associates, Inc., Red Hook, NY, Aug. 2012, pp. 481–496; also AIAA Paper 2012-4585.